

# Scale redundancy and soft gauge fixing in positively homogeneous neural networks

Rodrigo Carmo Terin<sup>1,\*</sup>

<sup>1</sup>*King Juan Carlos University, Faculty of Experimental Sciences and Technology,  
Department of Applied Physics, Av. del Alcalde de Móstoles, 28933, Madrid, Spain*

Neural networks with positively homogeneous activations exhibit an exact continuous reparametrization symmetry: neuron-wise rescalings generate parameter-space orbits along which the input–output function is invariant. We interpret this symmetry as a gauge redundancy and introduce gauge-adapted coordinates that separate invariant and scale-imbalance directions. Inspired by gauge fixing in field theory, we introduce a soft orbit-selection (norm-balancing) functional acting only on redundant scale coordinates. We show analytically that it induces dissipative relaxation of imbalance modes to preserve the realized function. In controlled experiments, this orbit-selection penalty expands the stable learning-rate regime and suppresses scale drift without changing expressivity. These results establish a structural link between gauge-orbit geometry and optimization conditioning, providing a concrete connection between gauge-theoretic concepts and machine learning.

## I. INTRODUCTION

Deep neural networks (DNNs) achieve remarkable empirical performance, yet the geometry of their parameter space remains only partially understood. In particular, optimization stability can depend strongly on learning rate, initialization scale, and internal parametrization choices, even when the realized input–output function is unchanged. This observation has motivated a broad effort to import ideas from statistical physics and field theory into deep learning, including large- $N$  expansions, diagrammatic techniques, and effective descriptions near criticality [1–8]. In particular, stability near the edge of chaos has been shown to be governed by structural constraints rather than task-specific details [6, 8–11].

A fundamental structural feature of many modern architectures is positive homogeneity of activation functions such as ReLU. Positive homogeneity implies that neuron-wise rescalings of incoming and outgoing weights can leave the network function invariant. This rescaling invariance is well known and has been exploited in several contexts. Scale-invariant optimization methods such as G-SGD explicitly operate in quotient-like parameter spaces induced by this symmetry [12], while weight-balancing procedures provide function-preserving repair flows that reduce internal imbalance without altering the realized mapping [13]. More generally, recent analyses have asized that parameter-space symmetries give rise to degeneracies and flat directions in the loss landscape [14].

The present work does not rediscover this invariance. Instead, we make its orbit structure explicit and treat neuron-wise rescaling as a gauge redundancy in parameter space. Under this viewpoint, parameter configurations related by positive diagonal rescalings form continuous equivalence classes (orbits) that represent the same function. The task loss is constant along these directions, implying the existence of flat gauge modes that are invisible at the level of the input–output mapping.

Neuron-wise scale invariance induced by positive homogeneity has been previously studied from multiple perspectives. Scale-invariant optimization methods such as G-SGD explicitly perform updates in positively scale-invariant spaces [12], while weight-balancing procedures construct function-preserving flows that reduce internal imbalance [13]. Permutation symmetries and other parameter-space degeneracies have also been shown to induce flat valleys and saddle structures in loss landscapes [14].

Moreover our approach differs in emphasis and construction. Rather than reparametrizing the optimization algorithm or applying explicit repair steps, we introduce a variational gauge-fixing functional that acts exclusively on the redundant scale coordinates while leaving gauge-invariant quantities untouched. This provides (i) an explicit orbit–slice decomposition of parameter space, (ii) a tunable conditioning mechanism integrated into the loss, and (iii) a diagnostic framework based on gauge coordinates that quantifies scale drift and stability boundaries. In this sense, the gauge-theoretic formulation serves not merely as terminology, but as a geometric principle organizing the role of reparametrization redundancy in optimization.

Interpreting rescaling invariance in orbit language enables us to introduce a simple variational gauge-fixing principle. We define explicit gauge coordinates associated with neuron-wise scale imbalance and construct a soft gauge-fixing

---

\* [rodrigo.carmo@urjc.es](mailto:rodrigo.carmo@urjc.es)

functional that acts only on these coordinates, leaving orbit invariants untouched. Unlike global regularizers such as weight decay, the proposed term does not penalize overall magnitude, and unlike batch normalization it does not modify the forward pass. It instead selects a canonical representative within each rescaling orbit. Therefore, our contribution is threefold:

- (i) We formalize neuron-wise rescaling as a continuous orbit structure in parameter space and identify explicit gauge coordinates that separate invariant and redundant directions.
- (ii) We introduce a soft gauge-fixing functional that acts exclusively on the redundant scale coordinates and prove the existence of a balanced representative on each orbit.
- (iii) We quantify the geometric impact of lifting these flat directions through stability-region diagnostics and scale-drift measurements, showing that gauge fixing expands the empirically stable learning-rate regime while preserving the realized function up to machine precision.

The emphasis of this work is therefore geometric rather than purely empirical. We do not claim large improvements in validation error in minimal tasks. Instead, we demonstrate that redundant rescaling directions modify the effective conditioning encountered by gradient descent, and that softly lifting them alters the stability boundary of optimization. This perspective complements existing work on scale-invariant optimization and weight-balancing flows. Whereas prior approaches either repair imbalance through explicit function-preserving updates [13] or reparametrize optimization in quotient spaces [12], we introduce a tunable variational gauge-fixing term that can be integrated directly into the training objective and whose effect can be diagnosed through orbit-based coordinates. In this sense, the gauge interpretation provides both a unifying geometric language and a practical conditioning mechanism.

The paper is organized as follows. Section II formalizes neuron-wise rescaling as a gauge redundancy and introduces gauge-adapted coordinates that separate invariant and redundant directions. Section III presents the norm-balancing functional and proves the existence of balanced representatives on each gauge orbit. Section IV derives the gradient-flow dynamics in gauge coordinates, showing that the proposed gauge-fixing term induces an explicit dissipative relaxation of the imbalance modes. Section V provides stability-region diagnostics, learning-rate stress tests, and scale-drift measurements validating the theoretical analysis. We conclude in Sec. VII with implications for deeper homogeneous architectures and optimization geometry. Detailed derivations of the gauge-coordinate gradients and the resulting flow equations are collected in App. A.

## II. REPARAMETRIZATION SYMMETRY AS GAUGE REDUNDANCY

We begin by identifying an exact continuous reparametrization symmetry in neural networks with positively homogeneous activation functions and interpreting it as a gauge redundancy in parameter space.

Consider a fully connected neural network with a single hidden layer and ReLU activation,

$$f(x) = W_2 \sigma(W_1 x + b_1) + b_2, \quad (1)$$

where  $\sigma(z) = \max(0, z)$  is applied componentwise,  $W_1 \in \mathbb{R}^{H \times d}$ ,  $b_1 \in \mathbb{R}^H$ ,  $W_2 \in \mathbb{R}^{m \times H}$ , and  $b_2 \in \mathbb{R}^m$ . In the experiments of Sec. V we consider the scalar-output case  $m = 1$ , but the symmetry structure discussed below holds more generally.

The ReLU function is positively homogeneous of degree one,

$$\sigma(\alpha z) = \alpha \sigma(z), \quad \alpha > 0. \quad (2)$$

Let  $D = \text{diag}(s_1, \dots, s_H)$  be a diagonal matrix with strictly positive entries. Define the parameter transformation

$$\begin{aligned} W_1 &\rightarrow DW_1, & b_1 &\rightarrow Db_1, \\ W_2 &\rightarrow W_2 D^{-1}, & b_2 &\rightarrow b_2. \end{aligned} \quad (3)$$

Using the homogeneity of the activation, one immediately finds

$$\begin{aligned} f(x) &\rightarrow W_2 D^{-1} \sigma(D(W_1 x + b_1)) + b_2 \\ &= W_2 \sigma(W_1 x + b_1) + b_2. \end{aligned} \quad (4)$$

so that the input-output mapping of the network is exactly invariant under the transformation (3). Equation (3) therefore generates a continuous family of parameter configurations that all represent the same function  $f(x)$ . The

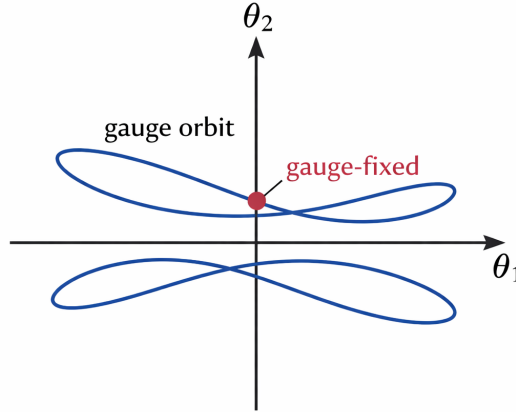


Figure 1: Gauge redundancy in parameter space. Neuron-wise positive rescalings generate continuous gauge orbits.

positive variables  $\{s_i\}$  label equivalence classes of physically indistinguishable parameterizations. Importantly, this symmetry does not arise from invariance of the data or of the task, but from an internal redundancy of the parameter space.

The structure is directly analogous to gauge symmetry in field theory. In gauge theories, multiple field configurations related by local transformations correspond to the same physical state. Here, the redundancy acts in parameter space rather than spacetime, but the mathematical structure is equivalent: the loss function is invariant along continuous orbits generated by (3). From the perspective of optimization, this symmetry implies the existence of flat directions in parameter space. Along these directions, the loss remains unchanged while the norms of individual parameter blocks can vary arbitrarily. Although such degeneracy does not alter the expressive power of the network, it allows large internal rescalings that can influence optimization dynamics.

In particular, gradient-based methods do not uniquely select a representative within each equivalence class. Parameters may therefore drift toward strongly imbalanced configurations in which adjacent layers differ significantly in scale, even though the realized function remains identical. This observation motivates the introduction of a gauge-fixing condition, in close analogy with gauge fixing in field theory, to remove the redundant directions and modify the geometry of the parameter space explored during training. The structure of this redundancy is illustrated schematically in Fig. 1, where different parameter configurations connected by neuron-wise rescaling correspond to the same network function. The Figure 1 above summarizes the central geometric picture: because of ReLU homogeneity, neuron-wise rescalings move parameters along continuous orbits that leave  $f(x)$  invariant. Optimization performed directly in parameter space can drift along these flat directions, changing internal scales without functional benefit. Gauge fixing introduces a preferred slice intersecting each orbit, thereby lifting the redundant directions in a controlled way.

### III. GAUGE FIXING BY NORM BALANCING

Having identified an exact reparametrization (gauge) redundancy in Sec. II, we now introduce a concrete gauge-fixing prescription. Our goal is to select, within each equivalence class of parameters representing the same function, a canonical representative that avoids extreme internal rescalings while leaving the realized mapping unchanged.

For the one-hidden-layer ReLU network in Eq. (1), the gauge transformation (3) rescales each hidden neuron independently:

$$z(x) = W_1 x + b_1 \in \mathbb{R}^H, \quad h(x) = \sigma(z(x)) \in \mathbb{R}^H, \quad (5)$$

as

$$z(x) \rightarrow Dz(x), \quad h(x) \rightarrow Dh(x), \quad (6)$$

while compensating this rescaling by transforming the outgoing weights  $W_2 \rightarrow W_2 D^{-1}$ . Although  $f(x)$  remains invariant, the internal parametrization can become strongly imbalanced: hidden activations may acquire large magnitude while the corresponding outgoing weights become small, or vice versa.

To remove this degeneracy we impose a balancing condition between the incoming and outgoing weights of each hidden neuron. Let  $W_{1,i} \in \mathbb{R}^d$  denote the  $i$ -th row of  $W_1$  (incoming weights of neuron  $i$ ), and let  $W_{2,:,i} \in \mathbb{R}^m$  denote the corresponding column of  $W_2$  (outgoing weights of neuron  $i$ ). We define the Euclidean norms

$$n_{1,i} \equiv \|W_{1,i}\|_2, \quad n_{2,i} \equiv \|W_{2,:,i}\|_2. \quad (7)$$

Under the gauge transformation (3),

$$n_{1,i} \rightarrow s_i n_{1,i}, \quad n_{2,i} \rightarrow \frac{1}{s_i} n_{2,i}, \quad (8)$$

so that the product  $n_{1,i} n_{2,i}$  is invariant while the ratio  $n_{1,i}/n_{2,i}$  can be tuned arbitrarily. A natural gauge condition therefore consists in fixing this ratio.

Rather than imposing a hard constraint, we introduce a soft gauge-fixing functional that penalizes scale imbalance multiplicatively:

$$\mathcal{G}(\theta) = \frac{1}{H} \sum_{i=1}^H [\log(n_{1,i} + \varepsilon) - \log(n_{2,i} + \varepsilon)]^2, \quad (9)$$

where  $\theta$  denotes all trainable parameters and  $\varepsilon > 0$  is a small constant introduced to ensure numerical stability when norms approach zero.

The functional (9) vanishes at perfectly balanced representatives. In fact, each rescaling orbit admits (at least) one balanced representative, obtained by an explicit neuron-wise rescaling: Assume  $n_{1,i}, n_{2,i} > 0$  for all hidden units. Consider the neuron-wise rescaling  $w_i \mapsto s_i w_i$ ,  $a_i \mapsto s_i^{-1} a_i$  with  $s_i > 0$ . For  $\varepsilon = 0$ , choosing  $s_i^* = \sqrt{n_{2,i}/n_{1,i}}$  yields  $n'_{1,i} = n'_{2,i} = \sqrt{n_{1,i} n_{2,i}}$  and therefore  $\mathcal{G}(\theta') = 0$ . For  $\varepsilon > 0$ , the choice  $s_i^* = \sqrt{(n_{2,i} + \varepsilon)/(n_{1,i} + \varepsilon)}$  minimizes  $\mathcal{G}$  along the orbit up to  $O(\varepsilon)$ . Training is performed by minimizing the modified objective

$$\mathcal{L}_{\text{total}}(\theta) = \mathcal{L}_{\text{task}}(\theta) + \lambda \mathcal{G}(\theta), \quad (10)$$

where  $\mathcal{L}_{\text{task}}$  is the task loss (mean-squared error in our experiments) and  $\lambda \geq 0$  controls the strength of gauge fixing. We emphasize that  $\lambda$  is not a gauge parameter in the field-theoretic sense. In gauge theory, changing a gauge parameter corresponds to selecting different representatives of the same physical configuration without changing physical predictions. Here, by contrast,  $\lambda$  is a penalty weight that modifies the optimization objective and therefore the training dynamics. The gauge structure refers solely to the exact rescaling equivalence  $\theta \sim \theta'$  induced by positive homogeneity. The functional  $\mathcal{G}$  selects a representative within each orbit, whereas  $\lambda$  controls how strongly this selection is represented during training.

The parameter  $\lambda$  interpolates between:

- $\lambda = 0$ : full gauge redundancy; optimization may drift along flat directions.
- small  $\lambda$ : weak lifting of the degeneracy, modifying the geometry of parameter space while leaving the task objective dominant.
- large  $\lambda$ : strong enforcement of scale balance, which may interfere with early optimization transients.

It is important to distinguish this construction from common normalization techniques. Batch normalization modifies activations and changes the forward pass. Weight decay penalizes large norms globally. In contrast, the present gauge-fixing term:

- acts exclusively on redundant scale directions,
- leaves the network function invariant under Eq. (3),
- targets relative imbalance rather than absolute magnitude.

In this sense, Eq. (9) plays a role analogous to gauge fixing in field theory: it selects a canonical representative within each equivalence class of parametrizations without modifying the physical content of the model.

Because the transformation (3) follows directly from the positive homogeneity of ReLU, it provides an exact diagnostic of the reparametrization symmetry. For any set of strictly positive scaling factors  $\{s_i\}$ , the transformed parameters  $\theta'$  represent the same input–output function as the original parameters  $\theta$ . To verify this explicitly, after

training we sample random positive scaling factors and apply the transformation (3) to the learned parameters. We then compute the mean absolute deviation between the original and transformed network outputs,

$$\Delta_{\text{inv}} \equiv \langle |f_{\theta}(x) - f_{\theta'}(x)| \rangle_x, \quad (11)$$

where the average is taken over a test set.

In our numerical experiments performed in double precision (NumPy default),  $\Delta_{\text{inv}}$  remains at the level of machine accuracy. Across 200 random gauge transformations we obtain

$$\begin{aligned} \min \Delta_{\text{inv}} &= 3.99 \times 10^{-18}, \\ \text{median} &= 6.68 \times 10^{-18}, \\ \max &= 1.14 \times 10^{-17}. \end{aligned}$$

These values are consistent with floating-point round-off error and confirm that the gauge symmetry is exact for the class of networks considered.

#### IV. GRADIENT-FLOW DYNAMICS IN GAUGE COORDINATES

The neuron-wise rescaling symmetry induced by positive homogeneity implies the existence of flat directions in parameter space. In this section we make this structure explicit at the level of training dynamics by deriving the gradient-flow equations in coordinates adapted to the gauge orbits. The result is a simple decomposition: the task loss acts as a driving force that can generate scale drift, while the gauge-fixing term induces an explicit dissipative relaxation of the gauge (imbalance) modes.

For the  $i$ -th hidden neuron we denote the incoming and outgoing weight blocks by

$$w_i \equiv W_{1,i} \in \mathbb{R}^d, \quad a_i \equiv W_{2,:i} \in \mathbb{R}^m, \quad (12)$$

with Euclidean norms

$$n_{1,i} \equiv \|w_i\|_2, \quad n_{2,i} \equiv \|a_i\|_2. \quad (13)$$

We define logarithmic norm coordinates (with  $\varepsilon > 0$  for numerical stability)

$$\alpha_i \equiv \log(n_{1,i} + \varepsilon), \quad \beta_i \equiv \log(n_{2,i} + \varepsilon), \quad (14)$$

and their sum/difference

$$u_i \equiv \alpha_i + \beta_i, \quad v_i \equiv \alpha_i - \beta_i. \quad (15)$$

Under neuron-wise rescaling  $w_i \rightarrow s_i w_i$ ,  $a_i \rightarrow s_i^{-1} a_i$  ( $s_i > 0$ ), one has  $u_i$  invariant while  $v_i \rightarrow v_i + 2 \log s_i$ . Thus  $v_i$  parametrizes the gauge (imbalance) direction along the orbit, whereas  $u_i$  is gauge-invariant. Training with the soft gauge fixing

$$\mathcal{L}_{\text{tot}}(\theta) = \mathcal{L}_{\text{task}}(\theta) + \lambda \mathcal{G}(\theta), \quad \mathcal{G}(\theta) = \frac{1}{H} \sum_{i=1}^H v_i^2 \quad (16)$$

induces the gradient-flow dynamics

$$\dot{w}_i = -\nabla_{w_i} \mathcal{L}_{\text{task}} - \lambda \nabla_{w_i} \mathcal{G}, \quad \dot{a}_i = -\nabla_{a_i} \mathcal{L}_{\text{task}} - \lambda \nabla_{a_i} \mathcal{G}, \quad (17)$$

where dot denotes derivative with respect to the (continuous) training time. A direct computation (given in App. A) yields

$$\nabla_{w_i} \mathcal{G} = \frac{2}{H} v_i \frac{w_i}{n_{1,i}(n_{1,i} + \varepsilon)}, \quad \nabla_{a_i} \mathcal{G} = -\frac{2}{H} v_i \frac{a_i}{n_{2,i}(n_{2,i} + \varepsilon)}. \quad (18)$$

Therefore the gauge-fixing contribution is purely radial in each block: it changes norms without rotating directions in weight space.

The induced dynamics for the gauge coordinate  $v_i$  can be written in closed form. Define the task-induced radial forces

$$F_i^{(1)} \equiv \langle \nabla_{w_i} \alpha_i, \nabla_{w_i} \mathcal{L}_{\text{task}} \rangle, \quad F_i^{(2)} \equiv \langle \nabla_{a_i} \beta_i, \nabla_{a_i} \mathcal{L}_{\text{task}} \rangle, \quad (19)$$

where  $\langle \cdot, \cdot \rangle$  denotes the Euclidean inner product. Then one obtains (App. A)

$$\dot{v}_i = -\left(F_i^{(1)} - F_i^{(2)}\right) - \frac{2\lambda}{H} v_i \left[ \frac{1}{(n_{1,i} + \varepsilon)^2} + \frac{1}{(n_{2,i} + \varepsilon)^2} \right]. \quad (20)$$

The first term acts as a driving force generated by the task loss and may produce scale drift along gauge orbits. The second term is strictly dissipative and provides an explicit damping rate

$$\kappa_i \equiv \frac{2\lambda}{H} \left[ \frac{1}{(n_{1,i} + \varepsilon)^2} + \frac{1}{(n_{2,i} + \varepsilon)^2} \right] > 0, \quad \dot{v}_i|_g = -\kappa_i v_i. \quad (21)$$

In particular, in the absence of task forcing ( $F_i^{(1)} = F_i^{(2)}$ ) the imbalance coordinate relaxes exponentially along each orbit,

$$v_i(t) = v_i(0) \exp\left(-\int_0^t \kappa_i(\tau) d\tau\right). \quad (22)$$

Near the balanced regime  $n_{1,i} \approx n_{2,i} \approx n_i$  one has the estimate

$$\kappa_i \approx \frac{4\lambda}{H} \frac{1}{(n_i + \varepsilon)^2}, \quad v_i(t) \approx v_i(0) \exp\left(-\frac{4\lambda}{H} \frac{t}{(n_i + \varepsilon)^2}\right). \quad (23)$$

Equation (20) makes precise the mechanism behind the observed suppression of scale drift: the gauge-fixing term adds an explicit dissipative potential along the gauge coordinates while leaving the input–output function invariant.

## V. EXPERIMENTS

We now assess the practical implications of the gauge-fixing term introduced in Sec. III. The experiments are deliberately minimal in order to isolate the structural effects of reparametrization symmetry, rather than to optimize task performance.

We consider a one-dimensional nonlinear regression task with target function

$$y(x) = \sin(2.5x) + 0.2 \cos(6x) + 0.1x + \eta, \quad (24)$$

where  $\eta$  is Gaussian noise with fixed variance. Training samples are drawn uniformly from  $[-2, 2]$ , while validation is performed on a wider interval  $[-3, 3]$ . Figure 2 illustrates the controlled regression setting. The training set is intentionally noisy, while validation is performed on a wider interval to probe generalization. This minimal setup is sufficient to expose optimization effects associated with reparametrization redundancy without conflating them with large-model capacity. All experiments use the single-hidden-layer ReLU network of Eq. (1) with width  $H = 20$ . The total loss (10) is minimized using plain gradient descent with fixed learning rate. Each configuration is trained for a fixed number of steps and averaged over multiple random seeds.

We first investigate the effect of the gauge-fixing strength  $\lambda$ . Figure 3 and Table I report the mean and standard deviation of training and validation mean-squared error (MSE) for several values of  $\lambda$ . Figure 3 shows that weak gauge fixing ( $\lambda \approx 0.05$ ) yields validation performance comparable to the baseline, whereas larger values of  $\lambda$  increase both the mean validation error and its variability across seeds. Quantitatively, Table I shows a mild optimum near  $\lambda = 0.05$  ( $0.5156 \pm 0.0044$ ) compared to the baseline  $\lambda = 0$  ( $0.5169 \pm 0.0038$ ), while strong gauge fixing substantially degrades generalization (e.g.  $\lambda = 0.50$ :  $0.63 \pm 0.16$ ). This supports the interpretation of  $\mathcal{G}(\theta)$  as a geometric conditioning term: useful when weak, but overly restrictive when too strong in this minimal setup. To further probe stability, we vary the learning rate while comparing baseline and gauge-fixed training at  $\lambda = 0.2$ . Table II reports the validation MSE together with a qualitative stability label.

At  $\text{lr} = 2 \times 10^{-2}$ , baseline training becomes unstable across seeds, while the gauge-fixed configuration remains stable. However, stability does not necessarily imply lower validation error at aggressive learning rates: for  $\lambda = 0.2$  the stable runs exhibit larger validation MSE than baseline training at smaller learning rates. This indicates that gauge fixing modifies the stability region of gradient descent, while the value of  $\lambda$  controls the trade-off between constraint strength and task optimization.

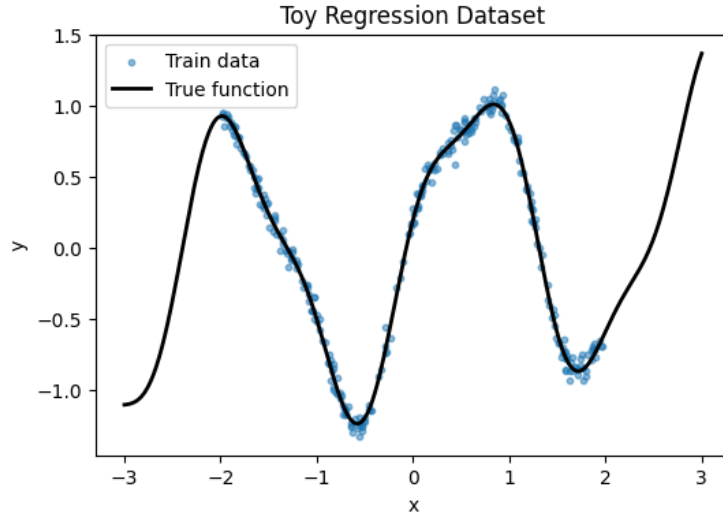


Figure 2: Toy regression dataset used in Sec. V. Training samples are drawn from  $[-2, 2]$  with additive Gaussian noise. The black curve shows the noiseless target function evaluated on the validation grid over  $[-3, 3]$ .

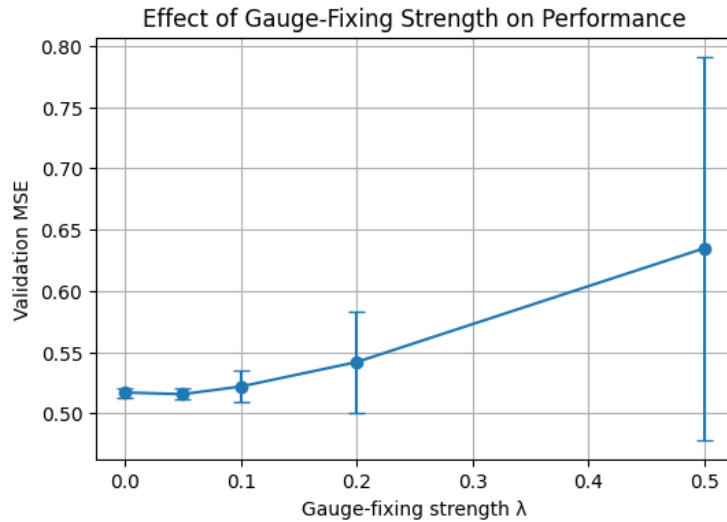


Figure 3: Validation mean-squared error as a function of the gauge-fixing strength  $\lambda$ . Each point corresponds to the mean over independent random seeds, with error bars given by the standard deviation.

$\lambda$	Train MSE	Validation MSE
0.00	$0.5358 \pm 0.0017$	$0.5169 \pm 0.0038$
0.05	$0.5312 \pm 0.0025$	$0.5156 \pm 0.0044$
0.10	$0.5281 \pm 0.0055$	$0.5218 \pm 0.0128$
0.20	$0.5240 \pm 0.0083$	$0.5418 \pm 0.0413$
0.50	$0.5177 \pm 0.0081$	$0.63 \pm 0.16$

Table I: Mean  $\pm$  standard deviation over independent random seeds.

Method	Learning rate	Validation MSE	Stability
Baseline	$5 \times 10^{-3}$	0.515360	Stable
Baseline	$1 \times 10^{-2}$	0.516924	Marginal
Baseline	$2 \times 10^{-2}$	0.521469	Unstable
Gauge-fixed ( $\lambda = 0.2$ )	$5 \times 10^{-3}$	0.524778	Stable
Gauge-fixed ( $\lambda = 0.2$ )	$1 \times 10^{-2}$	0.541801	Stable
Gauge-fixed ( $\lambda = 0.2$ )	$2 \times 10^{-2}$	0.567897	Stable

Table II: Learning-rate stress test. Gauge-fixed training remains stable at learning rates where baseline training becomes unstable in this toy setup.

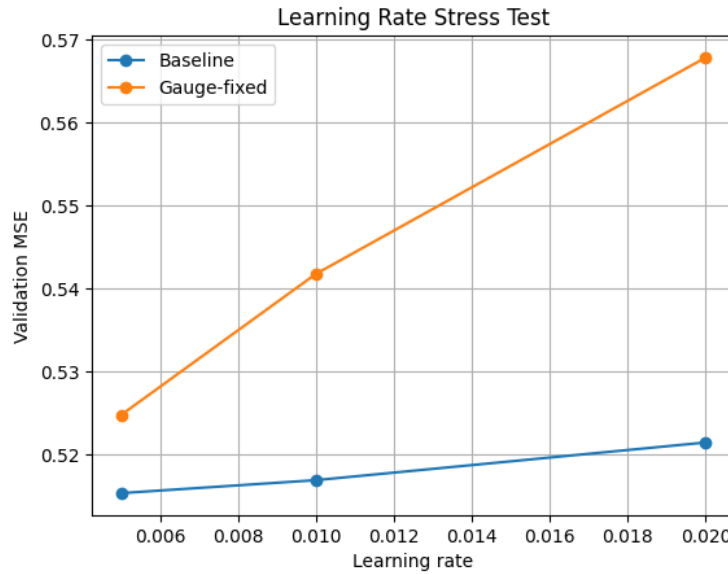


Figure 4: Learning-rate stress test comparing baseline and gauge-fixed training ( $\lambda = 0.2$ ). Gauge fixing expands the empirically stable learning-rate regime in this toy setup.

As a final consistency check, we apply random gauge transformations to trained models and compute the invariance error  $\Delta_{\text{inv}}$  defined in Eq. (11). The resulting distribution, shown in Fig. 5, remains at double-precision numerical accuracy ( $\mathcal{O}(10^{-17})$ ), confirming that gauge fixing does not alter the realized function.

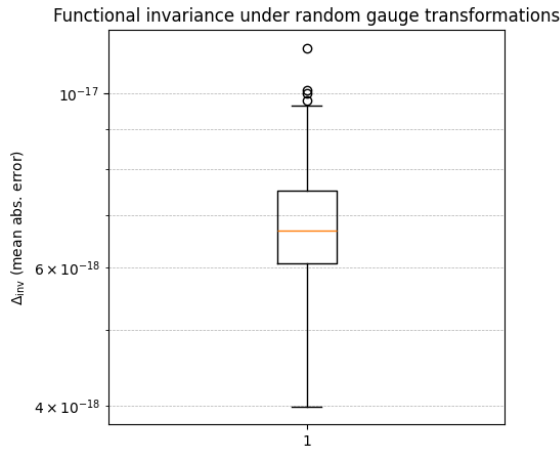


Figure 5: Functional invariance under random gauge transformations. Shown is a boxplot of the invariance error  $\Delta_{\text{inv}}$  defined in Eq. (11) across 200 random neuron-wise rescalings with  $s_i > 0$ . All values remain at double-precision numerical accuracy ( $\min 3.99 \times 10^{-18}$ , median  $6.68 \times 10^{-18}$ , max  $1.14 \times 10^{-17}$ ), confirming that the gauge transformations leave the network function unchanged up to machine precision.

## VI. DISCUSSION AND INTERDISCIPLINARY PERSPECTIVE

The experiments of Sec. V confirm that neural networks with positively homogeneous activations possess an exact continuous redundancy in parameter space and that softly lifting this redundancy modifies optimization dynamics without altering the realized function. Beyond the immediate numerical observations, this structure has conceptual implications in both directions: for optimization theory in computer science and for structural reasoning inspired by gauge theory in physics.

From the viewpoint of machine learning, neuron-wise rescaling invariance implies that the loss landscape contains continuous flat directions corresponding to redundant parametrizations. These directions enlarge the region explored by gradient descent without changing predictive performance. The imbalance coordinates  $v_i$  introduced in Sec. IV make these redundant modes explicit. In this coordinate system, the gauge-fixing term adds a strictly dissipative contribution  $v_i|_g = -\kappa_i v_i$ , revealing that part of the instability observed at large learning rates originates from unconstrained drift along symmetry directions rather than from model capacity or task complexity. In this sense, gauge fixing acts as a geometric conditioning mechanism: it reshapes the effective optimization geometry without modifying the model’s expressive power.

From the viewpoint of theoretical physics, the correspondence is structural rather than metaphorical. The symmetry arises from an exact positive homogeneity property and generates continuous orbits in parameter space. Gauge-invariant combinations (such as  $u_i$ ) remain untouched, while redundant coordinates ( $v_i$ ) can be isolated and controlled. The introduction of  $\mathcal{G}(\theta)$  parallels gauge fixing in field theory: it selects a representative on each orbit while preserving physical observables. Here the “observables” are the input–output functions  $f(x)$ . This establishes a concrete example in which gauge-theoretic language provides a mathematically precise description of optimization geometry outside traditional high-energy physics contexts.

The interdisciplinary value lies in the bidirectional transfer of structure. On the machine-learning side, orbit–slice decompositions clarify how reparametrization symmetries affect conditioning and stability. On the physics side, neural networks provide an accessible setting in which gauge redundancy, orbit geometry, and soft symmetry lifting can be studied in finite-dimensional systems with explicit dynamics. This interplay suggests that methods developed in one domain may inform the other: quotient-space optimization techniques in ML resemble gauge-fixed formulations in physics, while renormalization-inspired reasoning about scale flow may illuminate stability properties in deep networks.

Importantly, the primary role of  $\mathcal{G}(\theta)$  is geometric rather than regularizing. Weak gauge fixing modifies the stability boundary of gradient descent while preserving validation performance, whereas strong gauge fixing constrains the dynamics excessively. This trade-off reflects a familiar principle from gauge theory: fixing redundant directions improves mathematical control, but overconstraining can obscure useful dynamical freedom.

Although the present experiments are deliberately minimal, the underlying symmetry mechanism is general. Any architecture with positively homogeneous activations exhibits analogous scale redundancy. In deeper networks these symmetries propagate across layers, leading to richer orbit structures. Understanding these redundancies in geometric terms may offer a principled framework for analyzing conditioning, learning-rate stability, and parameter-space

curvature in modern architectures.

Generally our work shows that gauge-theoretic reasoning can function as a structural organizing principle in optimization theory. The symmetry is exact, the orbits are explicit, the gauge coordinates are computable, and the gauge-fixing term has a direct dynamical interpretation. This suggests that further development of symmetry-adapted coordinates, orbit-based diagnostics, and controlled symmetry lifting may provide a systematic bridge between high-energy physics concepts and large-scale learning systems.

## VII. CONCLUSION

We have identified an exact continuous reparametrization symmetry in neural networks with positively homogeneous activations and interpreted it as a gauge redundancy in parameter space. This symmetry generates flat directions along which the loss remains invariant, allowing internal scale redistribution without altering the realized function.

Inspired by gauge fixing in field theory, we introduced a norm-balancing functional that softly lifts this degeneracy while preserving the input–output mapping. The proposed gauge-fixing term does not restrict expressivity; rather, it selects a canonical representative within each equivalence class of parametrizations.

In a minimal regression experiment, we observed that weak gauge fixing leaves performance essentially unchanged, while strong gauge fixing can degrade validation error. However, the gauge-fixed configuration remains stable in regimes where baseline gradient descent becomes unstable, indicating that lifting redundant scale directions modifies optimization geometry in a nontrivial way.

These results suggest that part of the instability observed in homogeneous neural networks may be attributed to intrinsic reparametrization redundancy rather than solely to model capacity or optimizer choice. Controlling such redundancies provides a principled mechanism for reshaping the effective parameter landscape explored during training.

More broadly, this work shows that the analogy between neural network reparametrization and gauge symmetry can be made precise and operational. The symmetry is exact, the gauge orbits are explicit, and the gauge-fixing functional has a direct computational realization. Extending this perspective to deeper architectures and to other classes of homogeneous networks may offer further insight into the geometry of modern learning systems.

Lastly, here we address a parameter-space gauge redundancy induced by positive homogeneity: neuron-wise rescalings generate continuous orbits along which the network function is exactly invariant. Our norm-balancing term acts as a soft gauge fixing, selecting a canonical representative within each orbit and modifying optimization geometry without changing expressivity. This is complementary to a dynamical gauge invariance, as realized in our GINN framework, where Ward identities constrain fluctuation corrections and protect the critical stability boundary. A natural extension is to embed the present construction into a stochastic QFT-style effective action and promote architectures to slow variables evolving under a Markovian (Lindblad-type) dynamics in function space, thereby unifying parameter-space gauge fixing with symmetry-protected stochastic evolution.

### Appendix A: Derivation of the gradient-flow equations in gauge coordinates

In this appendix we provide the detailed derivation of the gradient-flow dynamics in the gauge-adapted coordinates introduced in Sec. IV.

#### 1. Preliminaries and notation

For each hidden neuron  $i$  we denote

$$w_i \equiv W_{1,i} \in \mathbb{R}^d, \quad a_i \equiv W_{2,:,i} \in \mathbb{R}^m, \quad (\text{A1})$$

and their norms

$$n_{1,i} \equiv \|w_i\|_2 = \sqrt{w_i^\top w_i}, \quad n_{2,i} \equiv \|a_i\|_2 = \sqrt{a_i^\top a_i}. \quad (\text{A2})$$

We define

$$\alpha_i \equiv \log(n_{1,i} + \varepsilon), \quad \beta_i \equiv \log(n_{2,i} + \varepsilon), \quad v_i \equiv \alpha_i - \beta_i, \quad u_i \equiv \alpha_i + \beta_i, \quad (\text{A3})$$

with  $\varepsilon > 0$ .

The gauge-fixing functional is

$$\mathcal{G}(\theta) = \frac{1}{H} \sum_{i=1}^H v_i^2, \quad \mathcal{L}_{\text{tot}} = \mathcal{L}_{\text{task}} + \lambda \mathcal{G}. \quad (\text{A4})$$

Gradient flow is defined by

$$\dot{\theta} = -\nabla_{\theta} \mathcal{L}_{\text{tot}}. \quad (\text{A5})$$

## 2. Gradients of the logarithmic norm coordinates

We first compute  $\nabla_{w_i} \alpha_i$ . Using  $\alpha_i = \log(n_{1,i} + \varepsilon)$  and the chain rule,

$$\nabla_{w_i} \alpha_i = \frac{1}{n_{1,i} + \varepsilon} \nabla_{w_i} n_{1,i}. \quad (\text{A6})$$

Since  $n_{1,i} = \sqrt{w_i^\top w_i}$ , one has

$$\nabla_{w_i} n_{1,i} = \nabla_{w_i} (w_i^\top w_i)^{1/2} = \frac{1}{2} (w_i^\top w_i)^{-1/2} \nabla_{w_i} (w_i^\top w_i) = \frac{1}{2n_{1,i}} 2w_i = \frac{w_i}{n_{1,i}}. \quad (\text{A7})$$

Substituting (A7) into (A6) yields

$$\nabla_{w_i} \alpha_i = \frac{w_i}{n_{1,i}(n_{1,i} + \varepsilon)}. \quad (\text{A8})$$

Similarly,

$$\nabla_{a_i} \beta_i = \frac{a_i}{n_{2,i}(n_{2,i} + \varepsilon)}. \quad (\text{A9})$$

Because  $v_i = \alpha_i - \beta_i$ , and  $\alpha_i$  depends only on  $w_i$  while  $\beta_i$  depends only on  $a_i$ , we obtain

$$\nabla_{w_i} v_i = \nabla_{w_i} \alpha_i = \frac{w_i}{n_{1,i}(n_{1,i} + \varepsilon)}, \quad \nabla_{a_i} v_i = -\nabla_{a_i} \beta_i = -\frac{a_i}{n_{2,i}(n_{2,i} + \varepsilon)}. \quad (\text{A10})$$

## 3. Gradients of the gauge-fixing functional

Since  $\mathcal{G} = \frac{1}{H} \sum_j v_j^2$  and  $v_j$  depends on  $(w_j, a_j)$  only,

$$\nabla_{w_i} \mathcal{G} = \frac{1}{H} \nabla_{w_i} (v_i^2) = \frac{2}{H} v_i \nabla_{w_i} v_i = \frac{2}{H} v_i \frac{w_i}{n_{1,i}(n_{1,i} + \varepsilon)}. \quad (\text{A11})$$

Likewise,

$$\nabla_{a_i} \mathcal{G} = \frac{1}{H} \nabla_{a_i} (v_i^2) = \frac{2}{H} v_i \nabla_{a_i} v_i = -\frac{2}{H} v_i \frac{a_i}{n_{2,i}(n_{2,i} + \varepsilon)}. \quad (\text{A12})$$

Equations (A11)–(A12) show that the gauge term acts purely radially in each weight block.

## 4. Gauge-only contribution to the block dynamics

Separating task and gauge parts in gradient flow,

$$\dot{w}_i = -\nabla_{w_i} \mathcal{L}_{\text{task}} - \lambda \nabla_{w_i} \mathcal{G}, \quad \dot{a}_i = -\nabla_{a_i} \mathcal{L}_{\text{task}} - \lambda \nabla_{a_i} \mathcal{G}, \quad (\text{A13})$$

the gauge-only components are obtained by dropping  $\mathcal{L}_{\text{task}}$ :

$$\dot{w}_i|_{\text{g}} = -\lambda \nabla_{w_i} \mathcal{G} = -\lambda \frac{2}{H} v_i \frac{w_i}{n_{1,i}(n_{1,i} + \varepsilon)}, \quad (\text{A14})$$

$$\dot{a}_i|_{\text{g}} = -\lambda \nabla_{a_i} \mathcal{G} = +\lambda \frac{2}{H} v_i \frac{a_i}{n_{2,i}(n_{2,i} + \varepsilon)}. \quad (\text{A15})$$

## 5. Dynamics of $\alpha_i$ and $\beta_i$

We now compute the time derivative of  $\alpha_i$  under gradient flow. By the chain rule,

$$\dot{\alpha}_i = \langle \nabla_{w_i} \alpha_i, \dot{w}_i \rangle. \quad (\text{A16})$$

For the gauge-only part, substitute (A8) and (A14):

$$\begin{aligned} \dot{\alpha}_i|_{\text{g}} &= \left\langle \frac{w_i}{n_{1,i}(n_{1,i} + \varepsilon)}, -\lambda \frac{2}{H} v_i \frac{w_i}{n_{1,i}(n_{1,i} + \varepsilon)} \right\rangle \\ &= -\lambda \frac{2}{H} v_i \frac{\langle w_i, w_i \rangle}{n_{1,i}^2(n_{1,i} + \varepsilon)^2} = -\lambda \frac{2}{H} v_i \frac{n_{1,i}^2}{n_{1,i}^2(n_{1,i} + \varepsilon)^2} = -\frac{2\lambda}{H} \frac{v_i}{(n_{1,i} + \varepsilon)^2}. \end{aligned} \quad (\text{A17})$$

Similarly, using

$$\dot{\beta}_i = \langle \nabla_{a_i} \beta_i, \dot{a}_i \rangle, \quad (\text{A18})$$

and substituting (A9) and (A15),

$$\begin{aligned} \dot{\beta}_i|_{\text{g}} &= \left\langle \frac{a_i}{n_{2,i}(n_{2,i} + \varepsilon)}, +\lambda \frac{2}{H} v_i \frac{a_i}{n_{2,i}(n_{2,i} + \varepsilon)} \right\rangle \\ &= +\lambda \frac{2}{H} v_i \frac{\langle a_i, a_i \rangle}{n_{2,i}^2(n_{2,i} + \varepsilon)^2} = +\frac{2\lambda}{H} \frac{v_i}{(n_{2,i} + \varepsilon)^2}. \end{aligned} \quad (\text{A19})$$

## 6. Closed dynamics for the gauge coordinate $v_i$

Since  $v_i = \alpha_i - \beta_i$ , we obtain for the gauge-only part

$$\begin{aligned} \dot{v}_i|_{\text{g}} &= \dot{\alpha}_i|_{\text{g}} - \dot{\beta}_i|_{\text{g}} \\ &= -\frac{2\lambda}{H} \frac{v_i}{(n_{1,i} + \varepsilon)^2} - \frac{2\lambda}{H} \frac{v_i}{(n_{2,i} + \varepsilon)^2} \\ &= -\frac{2\lambda}{H} v_i \left[ \frac{1}{(n_{1,i} + \varepsilon)^2} + \frac{1}{(n_{2,i} + \varepsilon)^2} \right]. \end{aligned} \quad (\text{A20})$$

Defining the damping rate

$$\kappa_i \equiv \frac{2\lambda}{H} \left[ \frac{1}{(n_{1,i} + \varepsilon)^2} + \frac{1}{(n_{2,i} + \varepsilon)^2} \right] > 0, \quad (\text{A21})$$

we can write  $\dot{v}_i|_{\text{g}} = -\kappa_i v_i$ .

Including the task loss, we introduce the task-induced radial forces

$$F_i^{(1)} \equiv \langle \nabla_{w_i} \alpha_i, \nabla_{w_i} \mathcal{L}_{\text{task}} \rangle, \quad F_i^{(2)} \equiv \langle \nabla_{a_i} \beta_i, \nabla_{a_i} \mathcal{L}_{\text{task}} \rangle, \quad (\text{A22})$$

so that

$$\dot{\alpha}_i = -F_i^{(1)} - \frac{2\lambda}{H} \frac{v_i}{(n_{1,i} + \varepsilon)^2}, \quad \dot{\beta}_i = -F_i^{(2)} + \frac{2\lambda}{H} \frac{v_i}{(n_{2,i} + \varepsilon)^2}. \quad (\text{A23})$$

Subtracting yields the full imbalance dynamics

$$\dot{v}_i = -\left( F_i^{(1)} - F_i^{(2)} \right) - \frac{2\lambda}{H} v_i \left[ \frac{1}{(n_{1,i} + \varepsilon)^2} + \frac{1}{(n_{2,i} + \varepsilon)^2} \right], \quad (\text{A24})$$

which is Eq. ( 20 ) in the main text.

For completeness, we also record the gauge-only contribution to  $u_i = \alpha_i + \beta_i$ :

$$\dot{u}_i|_{\text{g}} = \dot{\alpha}_i|_{\text{g}} + \dot{\beta}_i|_{\text{g}} = \frac{2\lambda}{H} v_i \left[ -\frac{1}{(n_{1,i} + \varepsilon)^2} + \frac{1}{(n_{2,i} + \varepsilon)^2} \right]. \quad (\text{A25})$$

Near the balanced regime  $n_{1,i} \approx n_{2,i}$  this term is subleading, so the dominant effect of gauge fixing is dissipative relaxation of the gauge coordinate  $v_i$ .

---

- [1] Sho Yaida. Non-gaussian processes and neural networks at finite widths. In *Proceedings of Machine Learning Research*, volume 107, pages 165–192, 2020.
- [2] Ethan Dyer and Guy Gur-Ari. Asymptotics of wide networks from feynman diagrams. In *International Conference on Learning Representations (ICLR)*, 2020.
- [3] Roberto Bondesan and Max Welling. The hints in your neural network: A quantum field theory view of deep learning. In *Proceedings of the 38th International Conference on Machine Learning*, volume 139, pages 1038–1048, 2021.
- [4] James Halverson, Anindita Maiti, and Keegan Stoner. Neural networks and quantum field theory. *Machine Learning: Science and Technology*, 2:035002, 2021. doi:10.1088/2632-2153/abeca3.
- [5] Harold Erbin, Vincent Lahoche, and Dine Ousmane Samary. Nonperturbative renormalization for the neural network–qft correspondence. *Machine Learning: Science and Technology*, 3:015027, 2022. doi:10.1088/2632-2153/ac4f69.
- [6] Daniel A. Roberts, Sho Yaida, and Boris Hanin. *The Principles of Deep Learning Theory*. Cambridge University Press, 2022.
- [7] Kevin T. Grosvenor and Ro Jefferson. The edge of chaos: Quantum field theory and deep neural networks. *SciPost Physics*, 12:081, 2022. doi:10.21468/SciPostPhys.12.3.081.
- [8] Rodrigo Carmo Terin. The GINN framework: a stochastic QED correspondence for stability and chaos in deep neural networks. 8 2025.
- [9] H. Sompolinsky, A. Crisanti, and H. J. Sommers. Chaos in random neural networks. *Physical Review Letters*, 61:259–262, 1988. doi:10.1103/PhysRevLett.61.259.
- [10] Ben Poole, Subhaneil Lahiri, Maithra Raghu, Jascha Sohl-Dickstein, and Surya Ganguli. Exponential expressivity in deep neural networks through transient chaos. In *Advances in Neural Information Processing Systems*, volume 29, pages 3360–3368, 2016.
- [11] C. G. Langton. Computation at the edge of chaos: Phase transitions and emergent computation. *Physica D*, 42:12–37, 1990. doi:10.1016/0167-2789(90)90064-V.
- [12] Qi Meng, Shuxin Zheng, Huishuai Zhang, Wei Chen, Qiwei Ye, Zhi-Ming Ma, Nenghai Yu, and Tie-Yan Liu.  $\mathcal{G}$ -sgd: Optimizing relu neural networks in its positively scale-invariant space. In *International Conference on Learning Representations (ICLR)*, 2019.
- [13] Lawrence K. Saul. Weight-balancing fixes and flows for deep learning. *Transactions on Machine Learning Research*, 2023.
- [14] Johanni Brea, Berfin Simsek, Bernd Illing, and Wulfram Gerstner. Weight-space symmetry in deep networks gives rise to permutation saddles, connected by equal-loss valleys across the loss landscape. *arXiv preprint*, 2019.